NUMERICAL MODELS OF LABORATORY STEEL CORROSION TESTS IN CONTACT WITH COMPACTED BENTONITE

F.J. Samper[1]*, L. Montenegro[1], A. Mon[1] y E. García[2]

[1]Centro de Investigaciones Científicas Avanzadas, ETS Ingenieros de Caminos, Canales y Puertos, Universidad de A Coruña, Campus Elviña s/n, 15071 A Coruña. e-mail: j.samper@udc.es, web: https://cica.udc.gal/es/grupo/gestion-sostenible-de-los-recursos-hidricos-y-del-suelo
[2]ENRESA Empresa Nacional de Residuos Radiactivos, S.A. C/ Emilio Vargas 7, 28043 Madrid: enga@enresa.es

RESUMEN. El acero y la bentonita compactada han sido propuestos como materiales de sellado en los sistemas multibarrera del almacenamiento geológico profundo (AGP) de residuos de alta actividad. La corrosión del contenedor puede causar alteraciones en la capa de sellado y modificar las propiedades de la bentonita como la porosidad, la permeabilidad y las capacidades de sorción e hinchamiento. En este trabajo se presentan modelos numéricos acoplados termo-hidro-químico-mecánicos de varios ensayos de corrosión realizados en laboratorio e in situ para estudiar las interacciones acero-bentonita bajo las condiciones de un AGP. Los resultados de los modelos de los ensayos de corrosión en las celdas pequeñas indican que: 1) La magnetita y el $Fe(OH)_2(s)$ son los principales productos de corrosión y compiten por la precipitación de Fe^{2+}; 2) Los productos de corrosión penetran pocos mm en la bentonita y; 3) Los resultados reproducen los datos de hierro medidos. Los resultados del modelo del ensayo de corrosión en celdas medianas indican que la magnetita no precipita en la bentonita como indican las observaciones experimentales.

ABSTRACT. Carbon steel and compacted bentonite have been proposed as candidate materials for the overpack and buffer, respectively, in the multi-barrier system of deep geological repositories for high-level radioactive waste. The corrosion of the carbon steel may induce buffer alterations, which could result in changes in bentonite parameters such as porosity, permeability and sorption and swelling capacities. Here we present coupled thermo-hydro-chemical-mechanical (THCM) models of several types of heating and hydration experiments on compacted bentonite (at laboratory and in situ scale) to study the interactions of iron-bentonite under repository conditions. The model results for the corrosion tests on small cells indicate that: 1) Magnetite and $Fe(OH)_2(s)$ are the main corrosion products which compete for Fe^{2+} precipitation; 2) The corrosion products penetrate a few mm into the bentonite; and 3) The numerical results fit the measured iron weight data. Model results of the corrosion tests on medium cells show no magnetite penetration in the bentonite as indicated by the experimental observations.

1.- Introduction

Carbon steel and compacted bentonite have been proposed for the overpack and buffer, respectively, in multi-barrier systems of deep geological repositories for high-level radioactive waste. The corrosion of the carbon steel may induce buffer alterations, which could alter bentonite parameters such as porosity, permeability and sorption and swelling capacities. Corrosion tests has been performed to ascertain the effects of the corrosion products in the bentonite (ENRESA, 2005, Torres et al., 2008).

CIEMAT performed two types of lab corrosion tests: 1) Corrosion tests on small cells (SC cells), with a length of 2.5 cm, which were designed to reproduce the repository conditions prevailing approximately 3,000 years after the emplacement of the waste when the bentonite is fully saturated and; 2) Corrosion tests on medium-size cells (FB cells), with a length of 10 cm, which were performed to simulate the operational and the early post-closure transient phases of the repository before achieving full saturation of the engineering barrier system (EBS) which is characterized by oxic to suboxic conditions. The tests were performed under anoxic conditions to mimic the conditions of the repository once the $O_2(g)$ is consumed.

De Wint and Torres (2009) reported a reactive transport model of some of these corrosion tests, which was performed with HYTEC. This model included iron hydroxide, goethite, hematite, iron, lepidocrite, magnetite, pyrite and siderite, but does not account for evaporation/condensation rate and bentonite swelling. The THCM model presented here accounts for bentonite swelling, evaporation and initial unsaturated conditions in the bentonite.

Here we present the numerical models of the SC and FB heating and hydration experiments performed by CIEMAT on compacted FEBEX (Full-scale Engineered Barrier Experiment) bentonite to study the interactions of iron-bentonite under repository conditions and analyse how such interactions affect the bentonite properties. These experiments were performed at several temperatures and on samples of different lengths. The experiments were modelled with INVERSE-FADES-CORE V2 (Zheng and Samper, 2004, 2005; Mon, 2017). The numerical models were started within the framework of the PEBS Project (Samper et al., 2014) and are being extended with the context of the EURAD-ACED Joint Project (Havlova e al., 2020).

2.- Laboratory corrosion tests

2.1. Corrosion tests on SC cells

The corrosion tests on small cells, SC cells, were

performed by CIEMAT in hermetic cylindrical cells. The cells contained 21 mm of compacted bentonite and 4 mm of carbon-steel powder (Fig. 1). The tests were performed with unsaturated compacted FEBEX bentonite (ENRESA 2000a, 2006a). The external cylindrical cell was made out of Teflon to prevent the deformation. Tests were performed at 25º, 50º and 100ºC. The bentonite blocks were compacted to a dry density of 1.65 g/cm3 and an initial gravimetric water content of 0.14. The hydration water was injected by a steel distribution plate at a pressure of 100 kPa. The duration of the tests ranged from 6 to 12 months. For the tests of 6 months, the reactive iron source was made of iron powder with a grain size of 450 mm and 60 mm and the hydration water was reduced granitic Grimsel water (reduced calcium bicarbonate type granite water from Switzerland). On the other hand, the tests with a duration of 12 months had a corrosion source made by carbon steel BS3 type in shavings of 2 mm; and they were hydrated with granitic and concrete waters.

The bentonite samples got fully saturated after 2 weeks. Most of the corrosion cells showed after the dismantling the following sequence of colours: white, greenish-blue, orange and black (Torres et al., 2008) which were interpreted as the stages of the transformation of $Fe(OH)_2(s)$ into magnetite. Several iron oxides and oxy-hydroxides such as goethite, lepidocrocite and magnetite were found in these experiments as a result of the transformation of $Fe(OH)_2(s)$. The penetration of the corrosion front into the bentonite was measured by determining the weight content of $Fe(OH)_2(s)$. Bentonite dry density, water content and saturation degree were measured at the end of the tests. There are no bentonite pore water concentration data at the end of the tests.

2.2. Corrosion tests on FB cells

The corrosion tests performed on medium-size cells, FB cells, were carried out at the CIEMAT facilities. The cells contain a cylindrical sample of compacted FEBEX bentonite with a height of 8.68 cm and a radius of 3.5 cm in contact with a cylindrical sample of Fe-powder with a height of 1.3 cm and a radius of 3.5 cm (Turrero et al., 2011). Both samples were emplaced into cylindrical hermetic cells with an internal diameter of 7 cm and an inner length of 10 cm (Fig. 1). The external cylindrical cell was made of Teflon to prevent the deformation of the cell. The tests were performed at anoxic conditions for durations ranging from 6 months to 13 years. All of them were mounted and run in the same way (heating and hydration), except for the FB6 cell, in which no hydration takes place. Cells were dismantled sequentially to study the evolution of the corrosion processes and evaluate how corrosion affects the properties of the bentonite. FB1 (6 months) and FB2 (15 months) cells were dismantled during the NFPRO project, FB3 (4.5 years) and FB4 (7 years) cells were dismantled within the PEBS project, while FB5 and FB6 are being dismantled within the EURAD project (Havlova et al., 2020).

The hydration system installed on the top of the cell injected granitic Grimsel water at a pressure of 600 kPa through a stainless steel tank at a controlled temperature of 22ºC. The tank was periodically weighed to check the water intake (Turrero et al., 2011). A temperature of 100ºC was imposed at the bottom of the cell through a plane stainless steel heater. The bentonite blocks were initially compacted to a dry density of 1.65 g/cm^3 and had an initial gravimetric water content of 0.14. The relative humidity and the temperature were measured on line during the experiments in two sensors located at 18 mm and 74 mm from the heater (Fig. 1). After dismantling of the FB cells, bentonite samples were taken to measure water content, dry density, exchanged cations and soluble salts. The chemical interactions of the bentonite and the corrosion products depend on the saturation of the Fe powder. The bentonite relative humidity plays an important role in Fe oxidation (Torres et al., 2013). Water vapour is the oxidizing agent. High relative humidity allows the formation of crystalline phases. Goethite was detected in the 6-month test (FB1 cell). Hematite precipitated in the 15-month test (FB2 cell). In the 4.5 (FB3), 7 (FB4) and 13 years (FB5) tests hematite, maghemite, goethite, lepidocrocite, akaganeite and magnetite were found at the bentonite-iron contact.

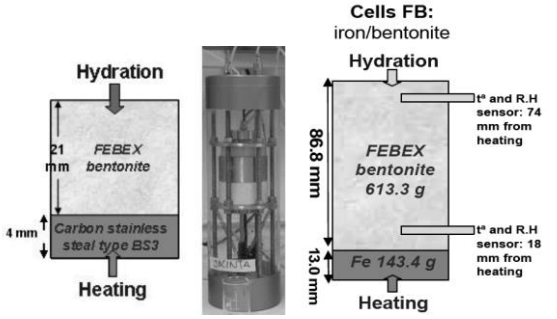

Fig. 1. Sketches of the corrosion tests on small cells (Torres et al., 2008) on the left and of the corrosion tests on medium-size cells (Turrero et al., 2011) on the right.

2.3. FEBEX in situ test

FEBEX (Full-scale Engineered Barrier Experiment) is a demonstration and research project dealing with the engineered barrier system of a high-level radioactive waste repository. FEBEX is based on the Spanish reference concept for radioactive waste disposal in crystalline rock (ENRESA, 2000). The canisters are emplaced in horizontal drifts and surrounded by a compacted bentonite clay barrier made of a Spanish bentonite from Cortijo de Archidona which is known as FEBEX bentonite. The FEBEX *in situ* test was performed in a gallery excavated in granite in the underground research laboratory of Grimsel, Switzerland. The main elements of the heating system are two heaters separated by 1 m. The heaters were designed to maintain a maximum temperature of 100ºC at the steel liner/bentonite interface. The bentonite barrier was made of blocks of highly compacted bentonite (Fig. 2). The test began in February 1997. Heater 1 was switched-off in

February 2002. After the emplacement of a shotcrete plug, the test continued operating until June 2015 when the barrier was fully dismantled (Fig. 2). Corrosion data were collected during the dismantling.

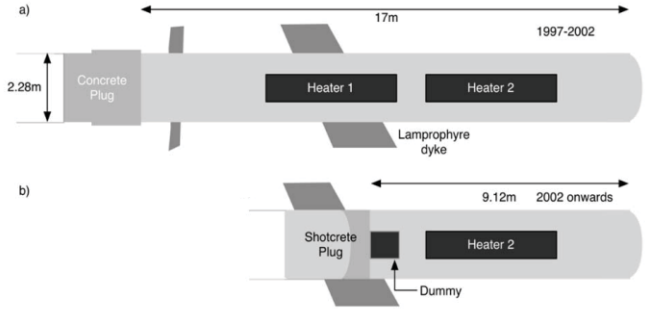

Fig. 2. General scheme of the FEBEX *in situ* test in the following periods: a) 1997 to 2002 and b) 2002 to 2015.

3.- THCM numerical model of the corrosion tests

THCM numerical models were performed for the corrosion tests performed on small cells at 25, 50 and 100ºC and corrosion tests on medium-size cells, FB3 and FB4 tests. The THCM numerical models include the bentonite and the Fe powder performed by a one-dimensional finite element mesh (Fig. 3). A liquid pressure of 100 kPa for the small cells and 600 kPa for the medium cells and a temperature of 22ºC were prescribed at the top of the cell. The temperature at the heater was fixed at 25º, 50º and 100ºC (Samper et al., 2014) for the small cells and 100ºC for the medium cells. The model simulates the heating and hydration during 180 days for the small cells and 1593 days for the FB4 test and 7 year for the FB5 tests. The main THM model parameters of the bentonite were taken from previous bentonite heating and hydration models (Zheng et al., 2010; ENRESA, 2000a, 2000b; Zheng and Samper, 2008). Some parameters such as the intrinsic permeability of the liquid of the bentonite were taken from other laboratory experiments on FEBEX bentonite (ENRESA, 2000a, 2000b). The parameters of the bentonite, such as the relative permeability of the liquid and the gas, and the thermo-osmotic permeability were taken from Zheng et al. (2010) and Zheng and Samper (2008). The vertical displacement was disabled at the top of the cell. The total stress was fixed to 250 kPa.

As an educated guess, the thermal and physical parameters of the Fe powder were taken from those of the Fe(s). The retention curve, the relative permeability of the liquid and the intrinsic and relative permeability of the gas for the Fe powder were assumed equal to those of the bentonite. The intrinsic permeability of the liquid in the Fe powder was assumed to be 100 times larger than that of the bentonite. It is assumed that there is no deformation in the Fe powder.

Bentonite has an initial porosity of 0.4 and an initial gravimetric water content of 0.14, which corresponds to a saturation of 57% and a suction of 1.27·105 kPa. The initial temperature of the cells is equal to 22ºC. The initial gas pressure is equal to the atmospheric pressure.

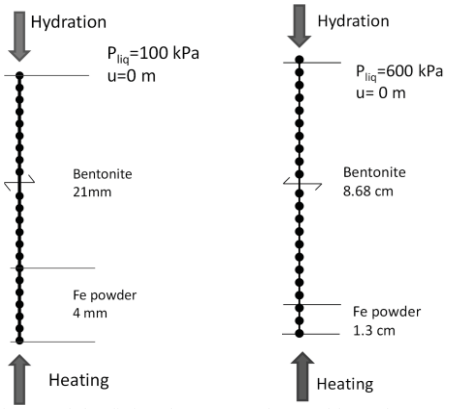

Fig. 3. Scheme of the finite element meshes and boundary conditions of the numerical model of the corrosion tests on small cells (left) and of the corrosion tests on medium-size cells (right) on the right.

A Neuman boundary condition was used for solute transport according to which solute flux is equal to the product of water flux times the solute concentration of inflow water. The diffusion coefficient in water, D_o, is assumed to be the same for all the dissolved species and equal to $2 \cdot 10^{-10}$ m^2/s. The diffusion coefficient in water for Cl^- was taken from Zheng et al. (2010) which is equal to $9 \cdot 10^{-11}$ m^2/s. The hydration water has the chemical composition of the Grimsel groundwater. Its chemical composition is listed in Table 1. The initial chemical composition of the bentonite pore water was taken from Fernández et al. (2001) (see Table 1).

The chemical system is defined in terms of the following primary species: H_2O, O_2(aq), H^+, Na^+, K^+, Ca^{2+}, Mg^{2+}, Fe^{2+}, HCO_3^-, Cl^-, SO_4^{2-} and SiO_2(aq). Tables 2 and 3 show the parameters and initial conditions for surface complexation and cation exchange reactions in the bentonite. Cation exchange reactions are not considered in the Fe powder. Surface complexation reactions are assumed to occur in the Fe powder to improve the convergence of the numerical solution. The initial volume fractions of the minerals are listed in Table 4. The bentonite contains initially 1% of calcite, 1% of quartz and 0.08% of gypsum.

The Fe powder is assumed to have the same diffusion coefficient, D_0 and porosity, ϕ, as the bentonite. The volume fraction of the Fe source is assumed to be 100% (Samper et al., 2016). The following secondary minerals are allowed to precipitate: gypsum, anhydrite, magnetite, goethite, siderite and $Fe(OH)_2$(s). The equilibrium constants of the homogeneous reactions, minerals, surface complexation and sorption are listed in Table 5.

H_2O is assumed to be the oxidizing agent of the canister similar to Lu et al. (2011) and Samper et al. (2016). Fe powder is treated as a porous mineral made of 100% of metallic iron, Fe(s). The corrosion reaction is given by:

$$Fe(s) + 2H^+ + 0.5O_2 \Leftrightarrow Fe^{2+} + H_2O$$

The following kinetic rate expression has been used for mineral dissolution/precipitation:

$$r_m = k_{25} e^{-\frac{Ea}{RT}} (\Omega_m{}^{\theta} - 1)^{\eta} \quad (1)$$

where r_m is the dissolution/precipitation rate (mol/m^2/s); is the kinetic rate constant (mol/m2/s) at 25ºC, Ω_m is the ratio between the ion activity product and the equilibrium constant (dimensionless) and θ and η are parameters of the kinetic law; $\frac{Ea}{RT}$ is the thermodynamic factor, which takes into account the apparent activation energy of the reaction, and Ea, and R and T are the gas constant and the absolute temperature, respectively.

Steel corrosion is kinetically controlled and takes place at a constant rate. Magnetite precipitation is also kinetically-controlled. The kinetic parameters for Fe(s) and magnetite were taken from De Windt and Torres (2009; 2010).

Table 1. Chemical composition of the initial porewater in the bentonite and the Grimsel hydration water.

	Initial bentonite porewater (Fernández et al., 2001)	Grimsel hydration water (Turrero et al., 2011)
Na^+	$1.3\cdot10^{-1}$	$3.7\cdot10^{-4}$
Ca^{2+}	$2.2\cdot10^{-2}$	$1.8\cdot10^{-4}$
Mg^{2+}	$2.3\cdot10^{-2}$	$1.6\cdot10^{-5}$
K^+	$1.7\cdot10^{-3}$	$2.2\cdot10^{-5}$
SO_4^-	$3.2\cdot10^{-2}$	$6.1\cdot10^{-5}$
Cl^-	$1.6\cdot10^{-1}$	$2.3\cdot10^{-5}$
SiO_2(aq)	$1.0\cdot10^{-4}$	$1.9\cdot10^{-4}$
HCO_3^-	$5.8\cdot10^{-4}$	$3.9\cdot10^{-4}$
Fe^{2+}	$6.6\cdot10^{-5}$	$1.8\cdot10^{-8}$
pH	7.72	9.7

Table 2. Site capacities (mol/L) of strong sites and weak #1 and weak #2 sites for FEBEX bentonite (Bradbury and Bayens, 1997, 2003).

Type of site	Bentonite	
	Surface complexes	Site capacity (mol/L)
S^S-OH	S^S-OH_2^+	0.015
	S^S-O^-	
	S^S-Fe^+	
	S^S-FeOH	
	S^S-$Fe(OH)_2^-$	
S^{w1}-OH	S^{w1}-OH_2^+	0.307
	S^{w1}-O^-	
	S^{w1}-Fe^+	
S^{w2}-OH	S^{w2}-OH_2^+	0.307
	S^{w2}-O^-	

Table 3. Initial concentrations of exchanged cations (in meq/100g) for FEBEX bentonite (Fernández et al., 2004).

Ca^{2+}	Mg^{2+}	Na^+	K^+	Fe^{2+}	CEC
34.62	34.01	31.18	1.94	0.5	102

Table 4. Initial mineral volume fractions (%) considered in the THCM model of the corrosion tests.

Bentonite		Fe powder	
Quartz	1	Iron	100
Calcite	1		
Gypsum	0.08		
Unreactive smectite	57.92		

Table 5. Chemical reactions and equilibrium constants for aqueous complexes and minerals (Wollery, 1992), protolysis constants for surface complexation reactions (Bradbury and Baeyens, 1997) and selectivity coefficients for cation exchange reactions (ENRESA, 2006b) at 25ºC.

Aqueous complexes	**Log K**
$CaCO_3(aq) + H^+ \Leftrightarrow Ca^{2+} + HCO_3^-$	7.0017
$CaHCO_3^+ \Leftrightarrow Ca^{2+} + HCO_3^-$	-1.0467
$CaSO_4(aq) \Leftrightarrow Ca^{2+} + SO_4^{2-}$	-2.1111
$CaOH^+ + H^+ \Leftrightarrow Ca^{2+} + H_2O$	12.850
$CO_2(aq) + H_2O \Leftrightarrow H^+ + HCO_3^-$	-6.3447
$CO_3^{2-} + H^+ \Leftrightarrow HCO_3^-$	10.3288
$KSO_4^- \Leftrightarrow K^+ + SO_4^{2-}$	-0.8796
$MgCO_3(aq) \Leftrightarrow Mg^{2+} + CO_3^{2-}$	-2.9789
$MgHCO_3^+ \Leftrightarrow Ca^{2+} + HCO_3^-$	-1.0357
$MgSO_4(aq) \Leftrightarrow Mg^{2+} + SO_4^{2-}$	-2.4117
$MgOH^+ \Leftrightarrow Mg^{2+} + OH^-$	-2.2100
$NaHCO_3(aq) \Leftrightarrow Na^+ + HCO_3^-$	-0.1541
$NaSO_4^- \Leftrightarrow Na^+ + SO_4^{2-}$	-0.8200
$NaCO_3^- \Leftrightarrow Na^+ + CO_3^{2-}$	-0.5144
$NaOH(aq) + H^+ \Leftrightarrow Na^+ + H_2O$	14.180
$OH^- + H^+ \Leftrightarrow H_2O$	13.9951
$H_3SiO_4^- + H^+ \Leftrightarrow 2H_2O + SiO_2(aq)$	9.8120
$HSO_4^- \Leftrightarrow H^+ + SO_4^{2-}$	1.9791
$HS^- + 2O_2(aq) \Leftrightarrow H^+ + SO_4^{2-}$	138.31
$Fe^{3+} + 0.5H_2O \Leftrightarrow H^+ + 0.25O_2 + Fe^{2+}$	-8.490
$FeHCO_3 \Leftrightarrow Fe^{2+} + HCO_3^-$	-2.050
$FeCO_3(aq) \Leftrightarrow Fe^{2+} + CO_3^{2-}$	-4.730
$FeCl^+ \Leftrightarrow Fe^{2+} + Cl^-$	0.1605
$FeCl^{2+} \Leftrightarrow Fe^{3+} + Cl^-$	0.8108
$FeOH^+ + H^+ \Leftrightarrow Fe^{2+} + H_2O$	10.895
$FeOH^{2+} + H^+ \Leftrightarrow Fe^{3+} + H_2O$	4.3815
$Fe(OH)_2(aq) + 2H^+ \Leftrightarrow Fe^{2+} + 2H_2O$	20.60
$Fe(OH)_3(aq) + 3H^+ \Leftrightarrow Fe^{3+} + 3H_2O$	12.172
$Fe(OH)_4^- + 4H^+ \Leftrightarrow Fe^{3+} + 4H_2O$	21.60
$Fe(OH)_2^+ + 2H^+ \Leftrightarrow Fe^{3+} + 2H_2O$	5.670
$Fe(SO_4)_2^- \Leftrightarrow Fe^{3+} + 2SO_4^{2-}$	-3.213
$FeSO_4(aq) \Leftrightarrow Fe^{2+} + SO_4^{2-}$	-2.20
$FeHSO_4^{2+} \Leftrightarrow Fe^{3+} + H^+ + SO_4^{2-}$	-1.540
$Fe_2(OH)_2^{4+} + 2H^+ \Leftrightarrow 2Fe^{3+} + 2H_2O$	7.2826
$KOH(aq) + H^+ \Leftrightarrow K^+ + H_2O$	14.46
$H_2(aq) + 0.5O_2 \Leftrightarrow H_2O$	46.10
$NaHSiO_3(aq) + H^+ \Leftrightarrow H_2O + Na^+ + SiO_2(aq)$	8.3040
$HSiO_3^- + H^+ \Leftrightarrow H_2O + SiO_2(aq)$	9.9525
$MgH_3SiO_4^+ + H^+ \Leftrightarrow 2H_2O + Mg^{2+} + SiO_2(aq)$	8.5416
Minerals	**LogK**
$Calcite + H^+ \Leftrightarrow Ca^{2+} + HCO_3^-$	1.8487
$Anhydrite \Leftrightarrow Ca^{2+} + SO_4^{2-}$	-4.3064
$Gypsum \Leftrightarrow Ca^{2+} + SO_4^{2-} + 2H_2O$	-4.4823
$Quartz \Leftrightarrow SiO_2(aq)$	-3.9993
$Magnetite + 6H^+ \Leftrightarrow 3Fe^{2+} + 0.5O_2(aq) + 3H_2O$	-6.5076
$Siderite + H^+ \Leftrightarrow Fe^{2+} + HCO_3^-$	-0.1920
$Goethite + 2H^+ \Leftrightarrow Fe^{2+} + 1.5H_2O + 0.25O_2(aq)$	-7.9555
$Fe(OH)_2(s) + 2H^+ \Leftrightarrow Fe^{2+} + 2H_2O$	13.9045
$Fe(s) + 2H^+ \Leftrightarrow Fe^{2+} + 2H_2O + 2OH^- + H_2(aq)$	-15.064
Surface complexation reactions	**LogK**
$\equiv S^SOH_2^+ \Leftrightarrow \equiv S^SOH + H^+$	-4.5
$\equiv S^SO^- + H^+ \Leftrightarrow S^SOH$	7.9
$\equiv S^sOFe^+ + H^+ \Leftrightarrow \equiv S^sOH + Fe^{2+}$	0.6
$\equiv S^sOFeOH + 2H^+ \Leftrightarrow \equiv S^sOH + Fe^{2+} + H_2O$	10.0
$\equiv S^sOFe(OH)_2^- + 3H^+ \Leftrightarrow \equiv S^sOH + Fe^{2+} + 2H_2O$	20.0
$\equiv S^{W1}OH_2^+ \Leftrightarrow \equiv S^{W1}OH + H^+$	-4.5
$\equiv S^{W1}O^- + H^+ \Leftrightarrow \equiv S^{W1}OH$	7.9
$\equiv S^{W1}OFe^+ + H^+ \Leftrightarrow \equiv S^{W1}OH + Fe^{2+}$	3.3
$\equiv S^{W2}OH_2^+ \Leftrightarrow \equiv S^{W2}OH + H^+$	-6.0
$\equiv S^{W2}O^- + H^+ \Leftrightarrow \equiv S^{W2}OH$	-10.5
Cation Exchange reactions	**$K_{Na\text{-}cation}$**
$Na^+ + X\text{-}K \Leftrightarrow K^+ + X\text{-}Na$	0.1456
$Na^+ + 0.5\ X_2\text{-}Ca \Leftrightarrow 0.5\ Ca^{2+} + X\text{-}Na$	0.3265
$Na^+ + 0.5\ X_2\text{-}Mg \Leftrightarrow 0.5\ Mg^{2+} + X\text{-}Na$	0.3766
$Na^+ + 0.5\ X_2\text{-}Fe \Leftrightarrow 0.5\ Fe^{2+} + X\text{-}Na$	0.5

The corrosion rate, r_c, in μm/year is calculated from:

$$r_c = \frac{r_m M_w b \sigma \emptyset}{f_v} \quad (2)$$

where r_m is the corrosion rate per unit mineral surface (mol/m^2/year); b is the iron thickness; V_m is the molar volume of iron; σ is the specific surface area; and f_v is the mineral fraction volume. The corrosion rate at 25ºC of the small and medium cells are assumed equal to 80 and 28 μm/year, respectively.

Table 6 shows the kinetic parameters. The values of the rate constants, k, were taken from De Wint and Torres (2009; 2010). The kinetic constant for the model of the SC tests at 50ºC was calibrated between the range proposed by De Windt and Torres (2009) in order to fit the measured iron weight data. This discrepancy is acceptable given the large uncertainty in the kinetic parameters and rate constants of iron phases.

Table 6. Kinetic parameters of Fe(s) and magnetite used in the THCM model of the corrosion tests (De Wint and Torres, 2009; 2010).

Mineral	Activation energy (kJ/mol)	$k_{25ºC}$ (mol/m^2/s)	θ	η	Specific surface (m^2/ m^3)
Fe (s)	11.0	$-4.0\cdot10^{-10}$	1	0	$2.15\cdot10^5$
Magnetite at 25ºC	20.0	$9.53\cdot10^{-11}$	0.1	1	$1.0\cdot10^5$
Magnetite at 50ºC	20.0	$2.00\cdot10^{-11}$	0.1	1	$1.0\cdot10^5$
Magnetite at 100ºC	20.0	$9.53\cdot10^{-11}$	0.1	1	$1.0\cdot10^5$

4.- Model results of the corrosion tests

4.1. Results for the SC corrosion tests

The computed water content is largest near the hydration boundary. It decreases towards the Fe powder-bentonite interface. The computed water content reproduces the measured value (Fig. 4). The bentonite becomes nearly saturated after 180 days. The computed temperature profile reaches steady state in a few minutes. Fig. 5 shows the computed temperature profiles for the corrosion tests on small cells at 25ºC, 50ºC and 100ºC.

Fig. 6 shows the spatial distribution of the concentration of dissolved Fe^{2+} at the end of the corrosion tests of carried out at 25, 50 and 100ºC. The general trend is similar for these three tests. The largest concentrations occur in the Fe powder. The concentrations in the bentonite are uniform with a local decrease near the interface. Fig. 7 shows the computed pH at the end of the tests after cooling for the tests at 25ºC, 50ºC and 100ºC. The computed pH are similar in all the tests.

Calcite and quartz dissolve in the bentonite with time (not shown here). Gypsum dissolves instantaneously in the bentonite while anhydrite precipitates near the heater after 7 days and then it dissolves (not shown here).

Fig 8 shows the computed iron corrosion at 25, 50 and 100ºC. The corrosion rate increases with temperature. The largest corrosion of Fe(s) corresponds to the test performed at 100ºC. Both magnetite and $Fe(OH)_2$(s) precipitate and compete for Fe^{2+} precipitation. The precipitation of magnetite is largest for the test at 100ºC and smallest for the test at 50ºC because the kinetic rate constant of magnetite is the smallest for 50ºC (Fig. 9).

Fig. 10 shows the spatial distribution of $Fe(OH)_2$(s) precipitation. $Fe(OH)_2$(s) does not precipitate in the test of 25ºC. The penetration front of the precipitation at 50ºC is larger than that at 100ºC. The numerical results fit the measured data of the iron weight for the tests performed at 50ºC and 100ºC and the results are similar to those of De Windt and Torres (2009) (Fig. 11).

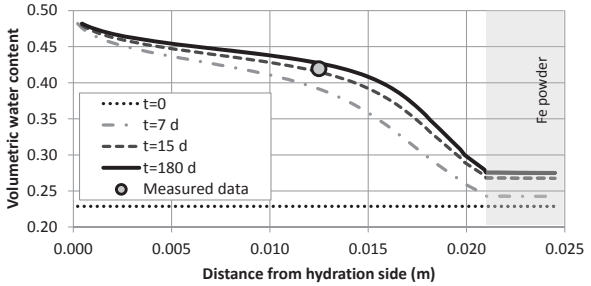

Fig. 4. Spatial distribution of the computed (lines) and the measured (Torres et al., 2008) (symbol) volumetric water content at selected times in the corrosion test on small cell a3 at 100ºC.

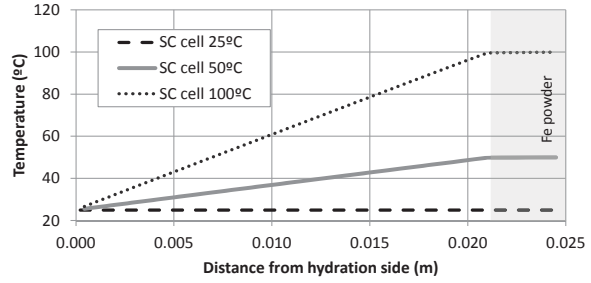

Fig. 5. Spatial distribution of the computed temperature in the corrosion test on small cells at 25ºC, 50ºC and 100ºC.

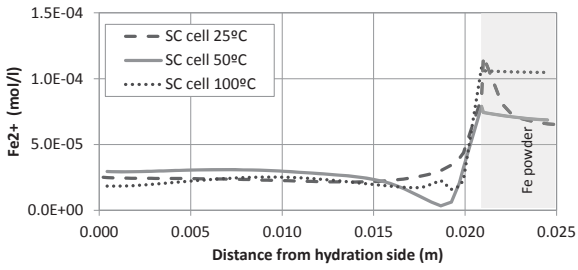

Fig. 6. Spatial distribution of the computed concentration of dissolved Fe^{2+} at the end of the corrosion tests (after cooling) in the small cells at 25, 50 and 100ºC.

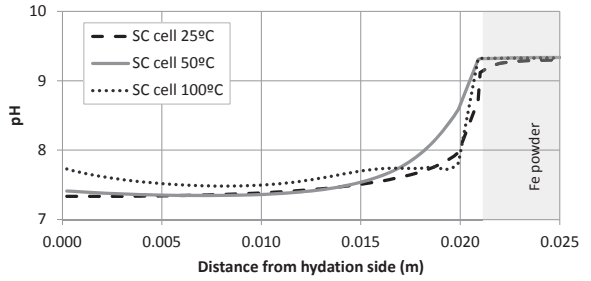

Fig. 7. Spatial distribution of the computed pH at the end of the corrosion tests (after cooling) in the small cells at 25, 50 and 100ºC.

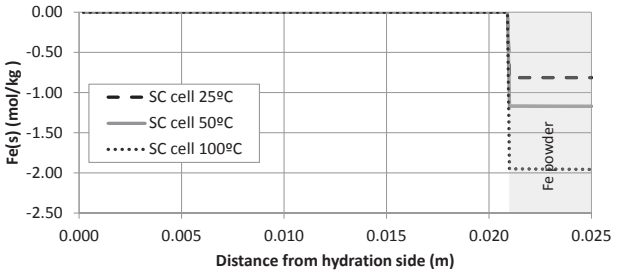

Fig. 8. Spatial distribution the computed cumulative dissolution for iron at the end of the corrosion tests (after cooling) in the small cells at 25, 50 and 100ºC.

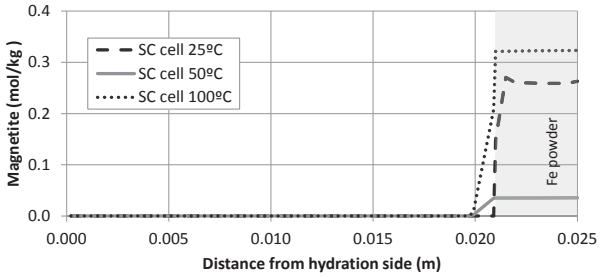

Fig. 9. Spatial distribution of the computed magnetite cumulative precipitation at the end of the corrosion tests (after cooling) in the small cells at 25, 50 and 100ºC.

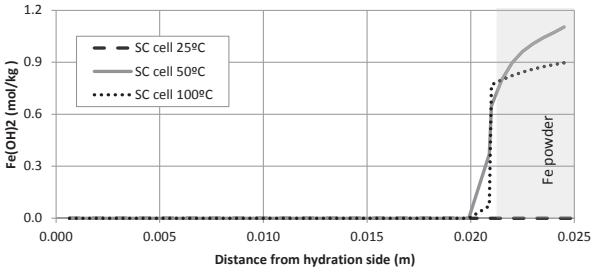

Fig. 10. Spatial distribution of the computed Fe(OH)2(s) cumulative precipitation at the end of the corrosion tests (after cooling) in the small cells at 25, 50 and 100ºC.

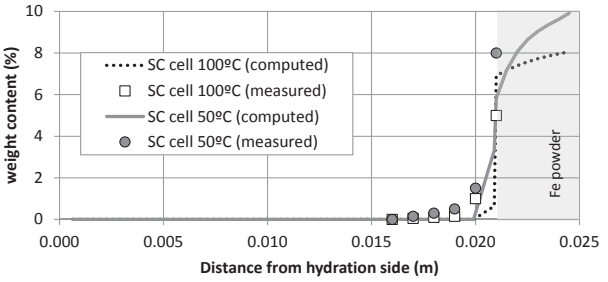

Fig. 11. Spatial distribution of the computed (lines) and the measured (symbols) iron weight (De Windt and Torres (2009)) at the end of the corrosion tests (after cooling) in the small cells at 25, 50 and 100ºC.

Model results show that S^{s}-OFe^{+} is the dominant sorbed species on the strong sites while S^{w2}-OH predominates on weak #2 sites and S^{w1}-OH and S^{w1}-OFe^{+} are the main sorbed species on the weak #1 sites. Fe^{2+} exchange is less relevant than Fe^{2+} sorption by surface complexation.

4.2. Results for the FB corrosion tests

The water intake in the first year is faster than that in the later years; 97% of the water enters during the first year. The total amount of water intake is equal to 0.083 L in 7 years.

Fig. 12 and Fig. 13 show the spatial distribution of the measured and the computed volumetric water content and porosity. The volumetric water content in the bentonite and Fe powder increases with time. It is largest in the bentonite near the hydration boundary. The water content near the hydration side is larger than that near the heater because the porosity increases near the hydration zone. Water evaporates near the heater. The vapour diffuses and condenses in colder locations. The computed volumetric water content is slightly smaller than the measured data near the hydration boundary. Near the Fe powder, however, the computed water content is larger than the measured values. The computed porosity increases to 0.488 from the initial value (0.40) in the bentonite near the hydration side. On the other hand, computed porosity is similar to the initial value in the bentonite near the Fe powder interface.

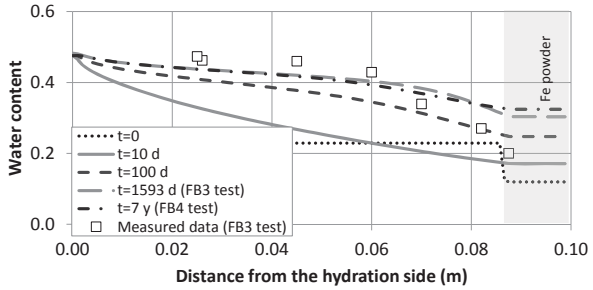

Fig. 12. Spatial distribution of the measured (symbols) (Turrero et al., 2011) volumetric water content at the end of the FB3 corrosion test and the computed (line) volumetric water contents at selected times in FB corrosion tests.

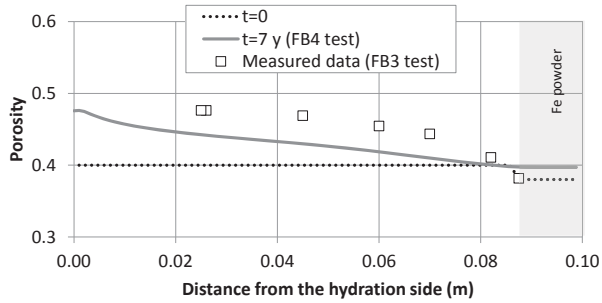

Fig. 13. Spatial distribution of the measured (symbols) (Turrero et al., 2011) porosity at the end of the FB3 corrosion test and the computed (line) porosities at the end of the FB3 and FB4 corrosion tests, which fully coincide.

Fig. 14 shows the evolution of the computed concentration of the dissolved Fe^{2+}. The dissolved concentration of Fe^{2+} decreases initially in the bentonite due to hydration and in the Fe powder due to magnetite precipitation. The concentration of Fe^{2+} at the end of the test (FB3 and FB4 corrosion tests) increases due to Fe(s)

corrosion. The computed pH is equal to 7.5 after the initial chemical equilibration. It decreases in the bentonite during the first 10 days, especially near the Fe powder. Then, pH increases to become similar to the initial pH, except in the Fe (s) where pH increases to 9.2 in the Fe powder (Fig. 15).

Computed gypsum dissolves initially in the bentonite and remains constant while computed anhydrite precipitates in the bentonite near the heater and at 1953 days (FB3 corrosion test) and at 7 years (FB4 corrosion test) anhydrite redissolves (not shown here). Computed calcite dissolved with time in the bentonite near the hydration side and near the Fe powder (not show here). Quartz dissolves in the bentonite near the Fe powder and precipitates punctually at the bentonite and Fe powder interface (not shown here).

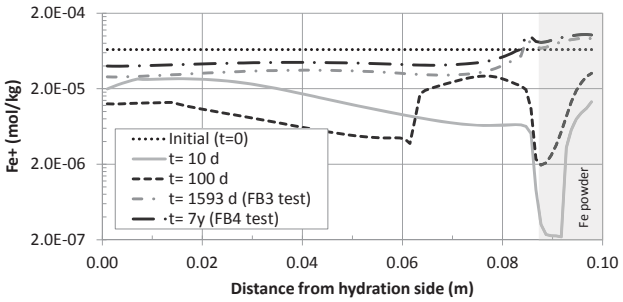

Fig. 14. Spatial distribution of the computed concentration of total dissolved Fe at selected times in the FB corrosion tests.

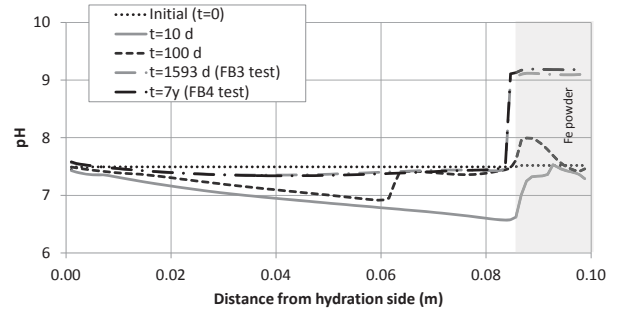

Fig. 15. Spatial distribution of the computed pH at selected times in the FB corrosion tests.

Fe(s) corrodes at a constant corrosion rate of 28 µm/year in the Fe powder. Computed magnetite precipitates in the Fe powder. A small amount of magnetite precipitates 2 mm into bentonite (Fig. 16). The experimental observations indicate that magnetite does not penetrate in the bentonite. Model results show no precipitation of siderite, goethite and $Fe(OH)_2(s)$. Fe^{2+} sorption takes place mostly in the strong and weak #1 sites.

5.- Conclusions and future work

We have presented coupled THCM models of several lab corrosion tests carried out by CIEMAT on: 1) Small cells with a length of 25 mm and a duration of 180 days; and 2) Medium-size cells (10 cm long) with a duration of 1593 days and 7 years. Thermal and hydrodynamic model results fit the general trends of the measured data in the bentonite in both corrosion tests.

Model results for the SC cells indicate that: 1) Magnetite and $Fe(OH)_2(s)$ are the main corrosion products which compete for Fe^{2+} precipitation; 2) The corrosion products penetrate a few mm into the bentonite; 3) The numerical results fit the measured iron weight data; 4) Fe^{2+} sorbes by surface complexation; and 5) Fe^{2+} exchange is less relevant than Fe^{2+} sorption by surface complexation.

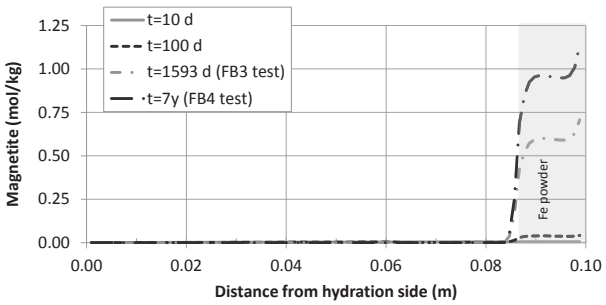

Fig. 16. Spatial distribution of the computed volume fraction of magnetite at selected times in the FB corrosion tests.

The chemical model results of the FB cells show that: 1) Magnetite precipitates in the Fe powder, but only in a small amount in the first 2 mm of the bentonite; and 2) There is no precipitation of siderite, goethite and $Fe(OH)_2(s)$. The experimental observations recorded by CIEMAT indicate that there is no magnetite penetration in the bentonite, which is consistent with the small amount of magnetite precipitation computed at the bentonite. However, model results do not reproduce the precipitation of hematite and magnetite/maghemite observed in the iron powder near the iron/bentonite interface.

The reactive transport model of the FB tests could be improved by considering:

- An initial aerobic phase and a later anaerobic corrosion stage.
- Additional corrosion products such as hematite, maghemite, Fe-phyllosilicates (cronstedtite and greenalite) and akaganeite.
- A time-varying corrosion rate for Fe powder depending on ambient conditions.
- A kinetically-controlled magnetite precipitation rate such as that reported by De Windt and Torres (2009) which was used for the model of the SC cells.
- Kinetically-controlled smectite dissolution
- The changes in porosity, permeability and diffusion coefficients caused by mineral dissolution/precipitation reactions

Work is in progress to perform a THCM model of the FEBEX in situ test by:

- Extending the previous THCM model of the FEBEX in situ test of Samper et al. (2018b) to account for redox processes, steel corrosion and the interactions of corrosion products and compacted

FEBEX bentonite.

- Implementing the conceptual geochemical model of steel corrosion in the FEBEX in situ test proposed by Hadi et al. (2019) including the aerobic and anaerobic corrosion phases.

Acknowledgements. The research leading to these results was funded by ENRESA through a Research Contract within the Work Package ACED of EURAD (European Joint Programme on Radioactive Waste Management of the European Union). The work was partly funded also by the Spanish Ministry of Economy and Competitiveness (Project PID2019-109544RB-I00) and the Galician Regional Government (Grant number ED431C2021/54 from "Consolidación e estruturación de unidades de investigación competitivas"). Corrosion tests were performed by CIEMAT. We acknowledge M.J. Turrero and E. Torres for their support and comments.

6.- References

Bradbury, M.H. and Baeyens, B., 1997. A mechanistic description of Ni and Zn sorption on Na-montmorillonite. Part II: modelling. J. Contam. Hydrol. 27, 223–248.

Bradbury, B. and Baeyens, B., 2003. Pore water chemistry in compacted resaturated MX-80 bentonite. J. Contam. Hydrol. 61, 329–338.

De Windt, L. and Torres, E., 2009. Modélisation d'expériences en cellule reproduisant les conditions THC d'une alvéole de déchets HAVL. Rapport Technique R201009LDEWI. Accord spécifique IRSN/ARMINES.

De Windt, L. and Torres, E., 2010. Interactions béton/argile sous gradient thermique et réhydratation : modélization d'experiénce en cellule. Rapport Technique R301110LDEWI. Accord spécifique IRSN/ARMINES.

ENRESA, 2000a. Full-scale engineered barriers experiment for a deep geological repository in crystalline host rock FEBEX Project. EUR 19147 EN, European Commission.

ENRESA, 2000b. Evaluación del comportamiento y de la seguridad de un almacenamiento de combustible gastado en una formación granítica. ENRESA Informe 49-1PP-M-15-01. Madrid, 2001.

ENRESA, 2005, Phenomenological description. Reference Concept (Spent Fuel-Carbon Steel Canister-Bentonite-Granite). NF-PRO Integrated Project. Deliverable D5.1.1. Part 1. Final version.

ENRESA, 2006a. Full-Scale Engineered Barriers Experiment: Updated Final Report. ENRESA Tech. Publ. PT 05-02/2006, 589 pp.

ENRESA, 2006b. FEBEX: Final THG modelling report. ENRESA Techn. Publ. PT 05-3/2006, 155 pp

Fernández, A.M., Cuevas, J. and Rivas, P., 2001. Pore water chemistry of the FEBEX bentonite. Mat. Res. Soc. Symp. Proc. 663,573-588

Fernández, A.M., Bayens, B., Bradbury, M. and Rivas, P., 2004. Analysis of pore water chemical composition of a Spanish compacted bentonite used in an engineered barrier. Phys. Chem Earth (29), 105-118.

Hadi, J., Wersin, P., Serneels, V., Greneche, J.-M., 2019. Eighteen years of steel-bentonite interaction in the FEBEX in situ test at the Grimsel Test Site in Switzerland. Clays and Clay Minerals 67(2), 111-131.

Havlova, V., Kiczka. M., Mendoza Miranda, A., Klajmon, M., Wersin, P., Jenni, A., Samper, J., Montenegro, L., Mon, A., Fabian, M., Osan, J., Dauzères, A., Jacques, D. (2020). Modelling of the steel-clay interface - approaches, first results and model refinements. Deliverable D2.6 of the HORIZON 2020 project EURAD. EC Grant agreement no: 847593.

Lu, C., Samper, J., Fritz, B., Clement and A., Montenegro, L., 2011. Interactions of corrosion products and bentonite: An extended multicomponent reactive transport model, Physics and Chemistry of the Earth 36, 1661–1668, doi: 10.1016/j.pce.2011.07.013.

Mon, A, 2017. Coupled thermo-hydro-chemical-mechanical models for the bentonite barrier in a radioactive waste repository. Ph. D. Dissertation. Universidad de A Coruña, Spain.

Samper, J., Mon, A., Montenegro, L., Pisani, B. and Naves, A., 2014. Report on testing multiple-continua THC(m) models with laboratory and large-scale tests Deliverable 3.4-1: PEBS Project, Project Deliverable 3.4-1. E.T.S.I. Caminos Canales y Puertos. Universidade de A Coruña.

Samper, J., Naves, A., Montenegro, L. and Mon, A., 2016. Reactive transport modelling of the long-term interactions of corrosion products and compacted bentonite in a HLW repository in granite: Uncertainties and relevance for performance assessment. Applied Geochemistry, 67, 42-51. DOI: 10.1016/j.apgeochem.2016.02.001.

Samper, J., Mon, A., Montenegro, L. (2018) A revisited thermal, hydrodynamic, chemical and mechanical model of compacted bentonite for the entire duration of the FEBEX in situ test. Appl. Clay Sci. 160, 58–70.

Torres, E., Turrero, M. J., Peña, J., Martín, P.L., Escribano, A., Alonso, U. and Villar, M.V., 2008. Deliverable 2.3.2 of component 2 NF-PRO project. Interaction iron-compacted bentonite: corrosion products and changes in the properties of the bentonite, 2008. CIEMAT

Torres, E., Turrero, M.J. and Escribano, A., 2013. Synthesis of corrosion phenomena at the iron/bentonite interface under unsaturated condictions. Thecnical Note CIEMAT/DMA/2G210/02/2013. PEBS Project.

Turrero, M. J., Villar, M. V., Torres, E., Escribano, A., Cuevas, J., Fernández, R., Ruiz, A. I., Vigil de la Villa, R. and del Soto, I., 2011. Deliverable 2.3-3-1 of PEBS Project. Laboratory tests at the interfaces, Final results of the dismantling of the tests FB3 and HB4, 2011. CIEMAT.

Wollery, T.J., 1992. EQ3/3. A software package for geochemical modeling of aqueous system: package overview and installation guide version 7.0. UCRL-MA-110662-PT-I, Lawrence Livermore National Laboratory, Livermore, California.

Zheng, L. and Samper, J., 2004. Formulation of the inverse problem of non-isothermal multiphase flow and reactive transport in porous media. Comput. Meth. Water Resour. XV, 1317–1327.

Zheng, L. and Samper, J., 2005. A dual continuum coupled multiphase flow model with mixed second order water transfer term for structured soils. Jornadas de la Zona no Saturada 2005, VII, 301-306.

Zheng, L. and Samper, J., 2008. A coupled THMC model of FEBEX mock-up test. Physics and Chemistry of the Earth 33, S486-S498

Zheng, L., Samper, J., Montenegro, L. and Fernández, A.M., 2010. A coupled model of heating and hydration laboratory experiment in unsaturated compacted FEBEX bentonite. Journal of hydrology 386, 80-94.